(Received 9 October 2025, Accepted 3 December 2025, Scheduled 15 December 2025)

Optimization of a Multi-Function Car-Roof Antenna Using Deep Learning Method

Dingwen Tan[1], Hexue Liu[2], Bing Xu[3,4], Xiaoming Liu[2], Shuo Yu[2], and Lu Gan[2,*]

[1] *China Construction Digital Technology Co., Ltd., Beijing 100161, China*
[2] *School of Physics and Electronic Information, Anhui Normal University, Wuhu 241002, China*
[3] *China Communication Information Technology Group Co., Ltd, Beijing 101300, China*
[3] *College of Computer Science and Technology, Harbin Engineering University, Harbin 150001, China*

ABSTRACT: This paper presents a dual-band car-roof antenna, which holds potential applications for 5G-MIMO, WLAN, and V2X. The proposed antenna is installed within a shark-fin room on the roof of vehicles. The proposed design consists of two parts, the diversity antenna and main antenna. To mitigate spatially selective fading and ensure coverage, both the diversity and main antennas have omnidirectional radiation patterns in the azimuth plane. To reach a multi-function design, deep learning method is used for optimization based on MATLAB-HFSS-API. Notably, the optimized antenna reaches a compact size of 27 mm × 30 mm × 2 mm. The antenna has two bands (−10 dB), including 3.35–3.75 GHz and 4.76–7.19 GHz, covering China Telecom (3.4–3.5 GHz), China Unicom (3.5–3.6 GHz), China Mobile (4.8–4.9 GHz), WLAN (5.15–5.35 GHz, 5.725–5.850 GHz), unlicensed Wi-Fi (5.850 GHz–5.895 GHz), V2X (5.895–5.925 GHz), and Wi-Fi 6E (5.925–7.125 GHz). The full-wave simulation results are in satisfactory consistency with the measured ones.

1. INTRODUCTION

Recently, autonomous driving has seen increased popularity. There has been a noticeable surge in the necessity for wireless systems that are deployed on various vehicles [1]. The implementation of 5G wireless technology, WLAN and other communication technologies is anticipated to play important roles in self-driving vehicles and Internet of Things (IoT), by facilitating the establishment of reliable connections [2]. For instance, 5G technology bears advantages of enhanced data rate, very low latency, increased reliability, and much larger user capacity [3, 4]. However, these existing wireless communication technologies have not yet completely deployed in Vehicle-to-Everything (V2X) network. One of the difficulties is that integrating multiple types of antennas within a confined shark-fin housing is a significant technical challenge, primarily due to physical size constraints and mutual coupling effects between adjacent antennas.

In recent years, various miniaturized multi-band car-roof antennas have been developed [5–14]. In [5], two monopoles are placed in a three-dimensional structure that intersect with each other, which perfectly fit the shark fin shell. However, there is no more room to host other antennas. Michel et al. proposed a low-profile printed antenna for vehicular communications, covering wireless standards in a wide frequency range (698–2690 MHz) that includes the LTE (Long Term Evolution) band [10]. This design does not cover the 5G band. A two element 2 × 2 linear array Yagi antenna operating at 3.5 GHz for low band 5G is presented in [11], exhibiting a bandwidth of 0.6 GHz. To accommodate more bands, further investigation is conducted. For instance, a multiple-input multiple-output (MIMO) antenna system with low profile is presented covering the entire frequency range of LTE, 5G, WLAN, and V2X between 700 MHz and 6 GHz [12]. Chen et al. reported a two-element V2X antenna array, which is interspersed between two LTE antennas and designed in shark-fin environment [13]. However, the antennas in [12] and [13] are too large with dimensions of 70 mm × 70 mm × 29 mm and 110 mm × 60 mm × 1.6 mm, respectively, hindering the integration of antennas for other frequency bands. To reduce the size, Kwon et al. developed a three-dimensional compact antenna containing V2X band [14], but its radiation pattern still needs further optimization to reach an omnidirectional one.

There are so many bands that must be considered, and the optimization of antenna in a shark-fin structure is a challenge. To achieve a satisfactory design, deep learning method for optimization is used in many antenna designs [15–18]. These works have demonstrated that deep learning methods bear much potential in antenna design and optimization, particularly for multi-band applications. The capability of optimization on complex structures with many parameters is also verified. For instance, Wu et al. reported the optimization of a dual-polarized high-isolation antenna using deep learning method [19]. The optimization was finished in about 22.7 hours, which is much more efficient through try-and-error method.

In this study, a car-roof antenna designed for 5G-MIMO, WLAN, and V2X applications is presented. To accommodate antennas into shark-fin housing and obtain the required antenna performance, deep learning method is used to optimize struc-

* Corresponding author: Lu Gan (lgan@ahnu.edu.cn).

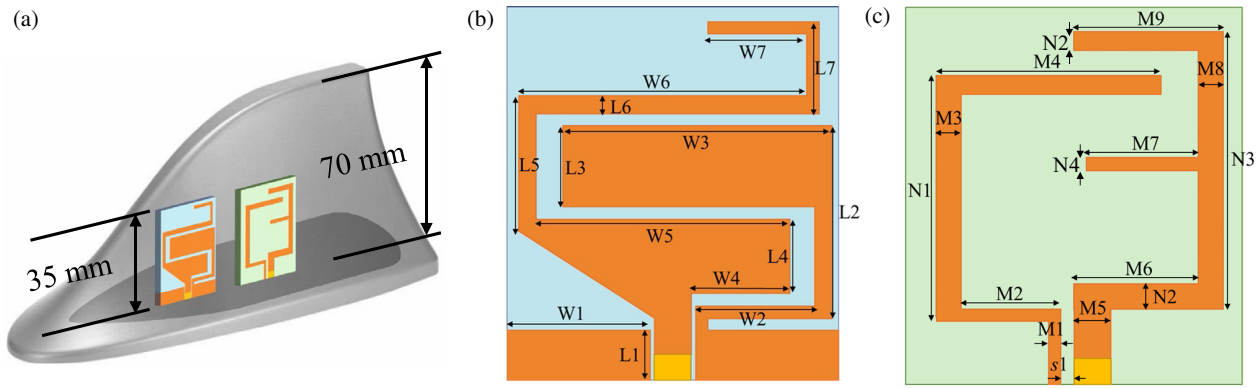

FIGURE 1. Configuration and dimension of the proposed combination antenna. (a) The shark-fin house, (b) the diversity antenna (c) the main antenna.

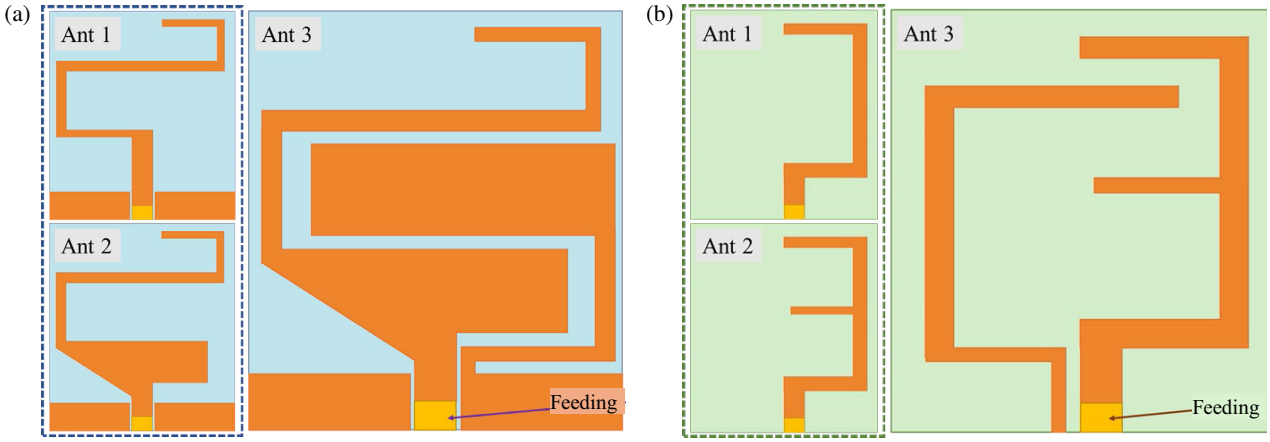

FIGURE 2. Evolution of the (a) diversity antenna and (b) main antenna.

ture, so that required performance is obtained. The remaining parts are organized as follows. Section 2 presents the design of the shark-fin antenna, including both initial structure and optimization strategies. Section 3 shows the measurement of the proposed antenna, and Section 4 concludes this work.

2. DESIGN OF ANTENNA IN SHARK-FIN AREA

2.1. Consideration of the Initial Structure

The purpose of this design is to host two antennas working in two different bands in a shark-fin room, as shown in Fig. 1(a). The antenna consists of two parts, the diversity antenna and main antenna, as shown in Fig. 1(b) and Fig. 1(c), respectively. The clear height of the shark-fin structure varies from around 35 mm to 70 mm. All the antennas are printed on FR-4 substrates ($\varepsilon_r = 4.4, \tan\delta = 0.02$) with a thickness of 2 mm.

The evolution of the diversity antenna and main antenna is shown in Fig. 2(a) and Fig. 2(b), respectively. Initially, the diversity antenna is designed as a meander line, acting as a monopole, labelled as Ant 1 in Fig. 2(a). Then, the part near the feeding point is revised labelled as Ant 2, as seen in Fig. 2(a). This revision is made trying to improve impedance matching. Lastly, the ground is extruded from the coplanar waveguide part to create more resonance, labelled as Ant 3 in Fig. 2(a).

For the main antenna, the initial design is also a meander monopole, labelled as Ant 1 in Fig. 2(b). A stub is added to Ant 1 to form an E-shaped radiation unit, labelled as Ant 2 in Fig. 2(b). Lastly, the ground is added to form Ant 3 as seen in Fig. 2(b).

2.2. Optimization Using Deep Learning Method

For most cases, optimization is conducted using try-an-error or parametric study. In this work, deep learning method is used to optimize the whole structure of the diversity and main antennas. A four-layer structure is shown in Fig. 3. This structure is revised from the method proposed in [19], where a dual-band antenna is optimized, and the success of using deep learning method is demonstrated. We have revised the input parameters to the central frequencies and their corresponding bandwidths, since the gain in this study is not the major concern. The bandwidth is defined as -10 dB reflection coefficients centered at the desired central frequency. Therefore, the central frequencies are defined as $f_1 = 3.5$ GHz and $f_2 = 6.0$ GHz. The expected bandwidths of the two bands are 0.4 GHz and 2.3 GHz, respectively.

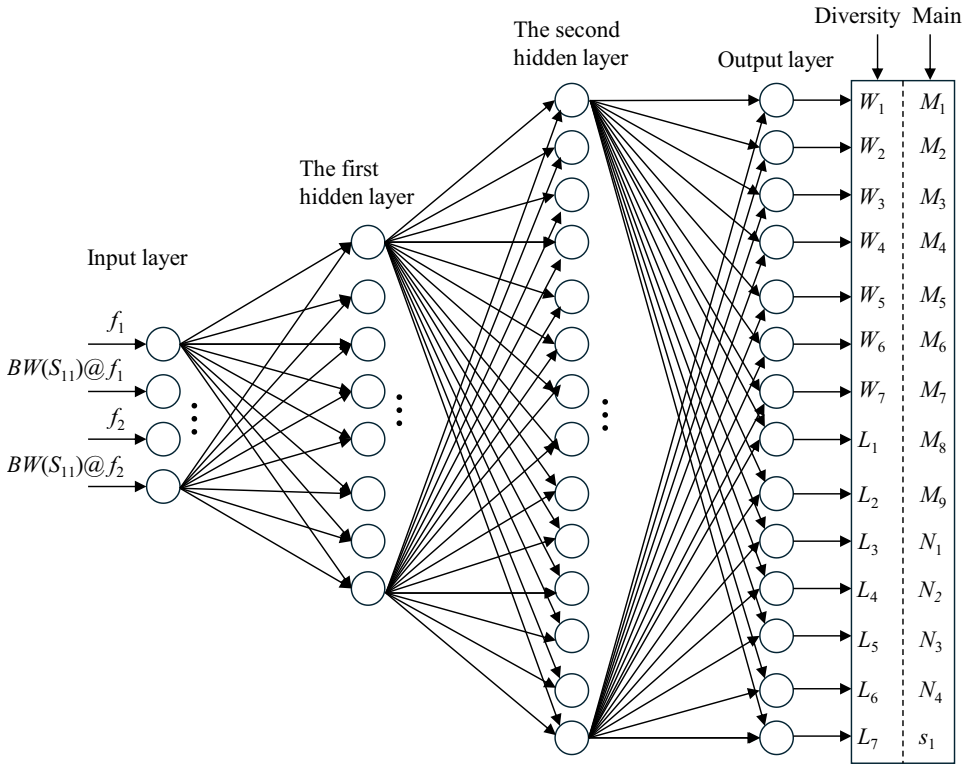

FIGURE 3. The four-layer optimization structure.

The propagation process of this model for the i-th neuron in the l-layer can be represented as

$$z_i^l = \sum_{j=1}^{N_l - 1} w_{i,j}^l a_j^{l-1} \tag{1}$$

where z_i^l and a_j^l are the linear results and nonlinear activation output of the i- and j-neurons in the l-layer, respectively; $w_{i,j}^l$ is the connection weight from the j-neuron in the $(l-1)$-layer to the i-neuron in the l-layer; N_l is the number of neurons in the l-layer. So one has

$$a_i^l = f\left(z_i^l\right) \tag{2}$$

with the activation function $f(z)$ defined as

$$f\left(z\right) = \frac{1}{1 + \mathrm{e}^{-z}} \tag{3}$$

In this design, we did not use the back propagation model. This is because the structure parameters are not too large in number, and the bounds of the structural parameters are initially well defined empirically. Alternatively, derivative-free optimization (DFO) method is used for such type of low-dimension problem. However, it is noted that for high-dimension problems, DFO method is less efficient, and we are trying to further investigate the training model with back propagation to be competent for more complicated structure. The difference between the predicted and desired values is defined as the loss function

$$\delta\left(a_i^{\text{out}}, a_i^{\text{in}}\right) = \frac{1}{Q} \sum_{i=1}^{Q} \left(a_i^{\text{out}} - a_i^{\text{in}}\right)^2 \tag{4}$$

where Q is the number of neurons in the input layer.

The lower bounds and upper bounds of each structural parameter are listed in Table 1. The upper bond of each parameter is set to ensure that the maximal size of the antenna must be hosted in the shark-fin room. By using the MATLAB-HFSS-API, simulation and optimization are conducted. The strategies follow that in [19]. The simulated results of Ant 1 and Ant 2 for both diversity and main antennas are based on the lower bound values. The optimized results are plotted in Fig. 4.

The diversity antenna is printed on a 2 mm thick FR-4 substrate. The feed line uses a 50 Ω coplanar waveguide (CPW) design for impedance matching. It can be seen from Fig. 4(a) that the diversity antenna can resonate around 3.19 GHz, 3.58 GHz, 4.97 GHz, and 5.9 GHz. The proposed diversity antenna can cover two wide bands, 3.02–3.81 GHz and 4.75–7.29 GHz. To shed some light on the resonance, the current distribution is plotted in Fig. 5. The resonances can be clearly seen from the current distribution.

The main antenna is also printed on an FR-4 substrate with a thickness of 2 mm, which can generate two resonances at 3.6 GHz and 4.9 GHz, respectively. The overall size of the proposed main antenna is $27 \times 30 \times 2$ mm, which can cover two bands of 3.35–3.75 GHz and 4.73–7.20 GHz. To further verify the working principle of the main antenna, we present the current distributions at three resonance points at 3.53 GHz, 5.28 GHz, and 6.26 GHz, as shown in Fig. 6. Also, the resonances can be seen from the current distribution.

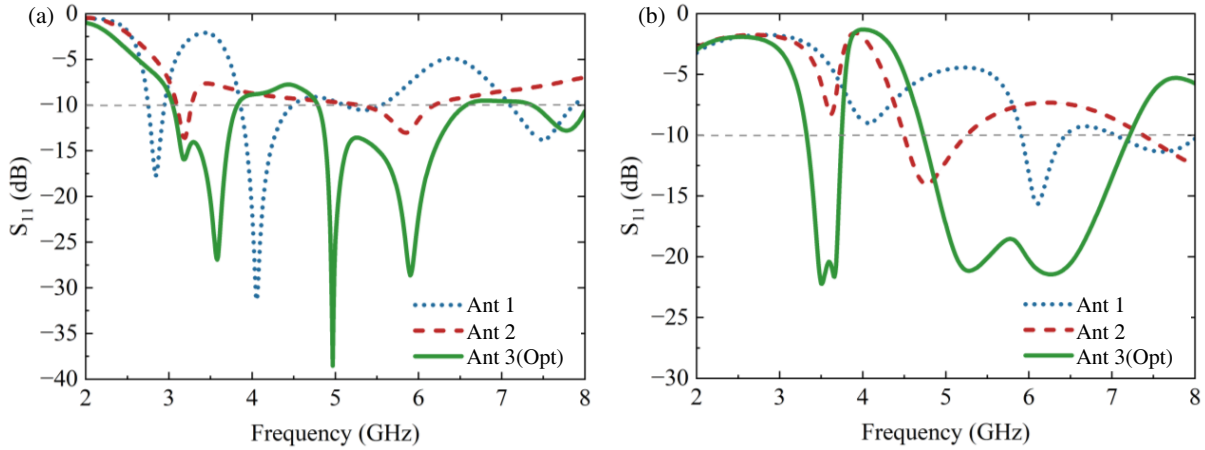

FIGURE 4. The optimized S_{11} for the (a) diversity antenna, and (b) main antenna.

TABLE 1. Optimized variables of the structural parameters (unit: mm).

Diversity antenna	Variables	$W1$	$W2$	$W3$	$W4$	$W5$	$W6$	$W7$
	Lower bound	10	9	20	7.5	19	22	7.5
	Upper bound	12	11	22	8.5	21	24	9.5
	Optimized	11.6	10.0	21.8	8.0	20.6	23.4	8.0
	Variables	$L1$	$L2$	$L3$	$L4$	$L5$	$L6$	$L7$
	Lower bound	3	15	6	6	10	1	7
	Upper bound	5	17	7	7	11	2	8
	Optimized	4.0	15.5	6.5	6.0	11.0	1.5	7.5
Main antenna	Variables	$M1$	$M2$	$M3$	$M4$	$M5$	$M6$	$M7$
	Lower bound	0.5	7	1	16	2	8	8
	Upper bound	1.5	9	2	20	3	10	10
	Optimized	1	8	2	18	3	10	9
	Variables	$M8$	$M9$	$N1$	$N2$	$N3$	$N4$	$s1$
	Lower bound	1	10	16	2	16	1	1
	Upper bound	2	14	22	3	24	2	2
	Optimized	2	12	19.5	2	22	1.5	1.5

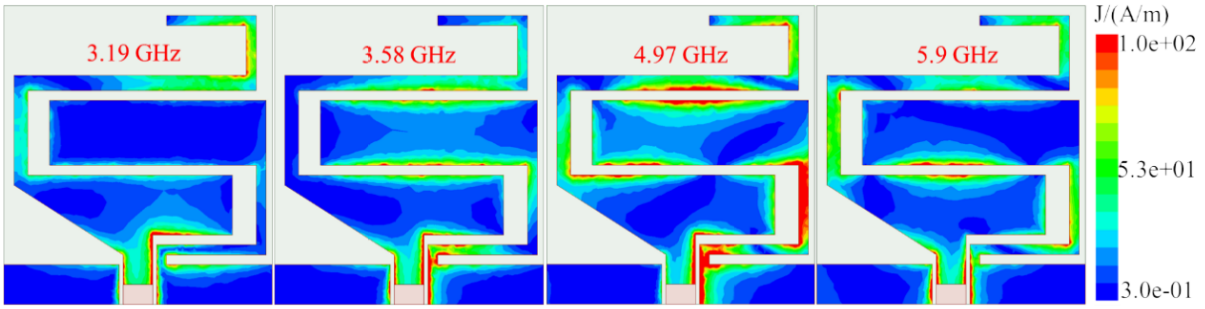

FIGURE 5. Current distribution of the diversity antenna at different resonance points.

3. FABRICATION AND MEASUREMENT

To verify the design of the proposed antenna, a prototype was built as shown in Fig. 7. Considering the effect of a car roof, the antenna is placed above a metal disc with a radius of 500 mm. The S-parameter of the antenna was measured using a vector network analyzer (VNA, Ceyear AV3672D), and the far-field properties such as radiation pattern, gain, and efficiency were tested in an anechoic chamber. Before the measurement, the VNA was calibrated using a standard short-load-open-thru (SLOT) method with a 3.5 mm calibration kit. It is noteworthy

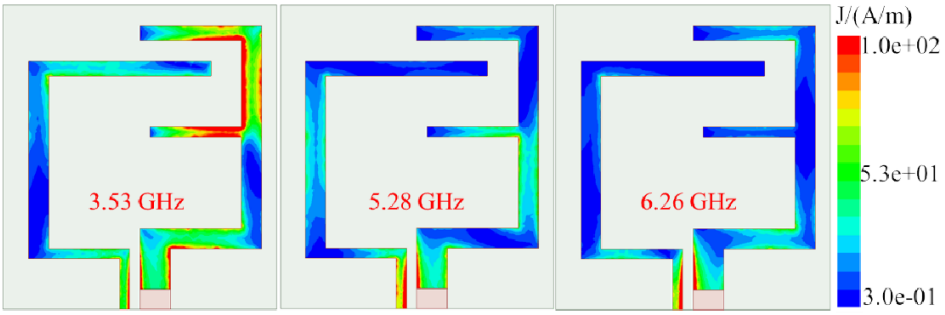

FIGURE 6. Current distribution of the main antenna at different resonance points.

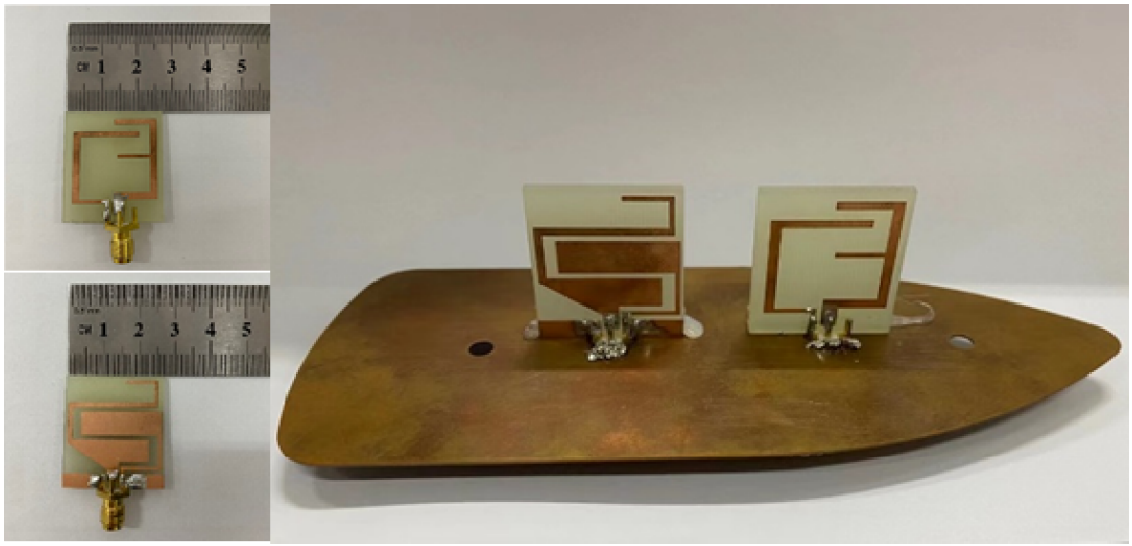

FIGURE 7. Photograph of the fabricated antenna.

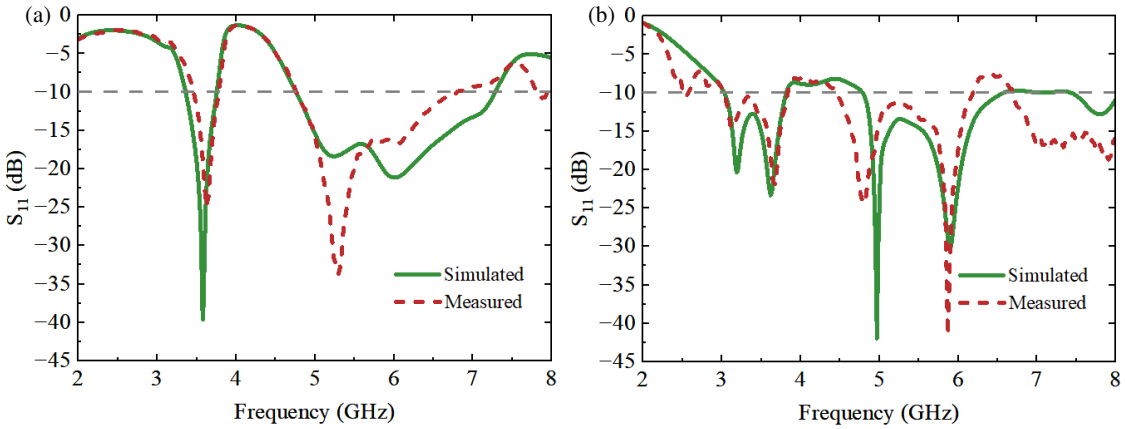

FIGURE 8. Comparison of simulated and measured results. (a) The main antenna. (b) The diversity antenna.

that the reflection coefficient and far-field radiation parameters are derived from measurements conducted with both antennas soldered. Each individual antenna was tested when the other antenna terminated with 50 Ω loads.

Figure 8 shows the simulated and measured reflection coefficients of the diversity and main antennas. Both diversity and main antennas provide −10 dB impedance bandwidths of 3.35–3.75 GHz and 4.76–7.19 GHz covering China Telecom (3.4–3.5 GHz), China Unicom (3.5–3.6 GHz), China Mobile (4.8–4.9 GHz), WLAN (5.15–5.35 GHz, 5.725–5.850 GHz), unlicensed Wi-Fi (5.850 GHz–5.895 GHz), V2X (5.895–5.925 GHz), and Wi-Fi 6E (5.925–7.125 GHz). The simulation results are in excellent concurrence with the measured ones. The slight differences between simulation and measurement

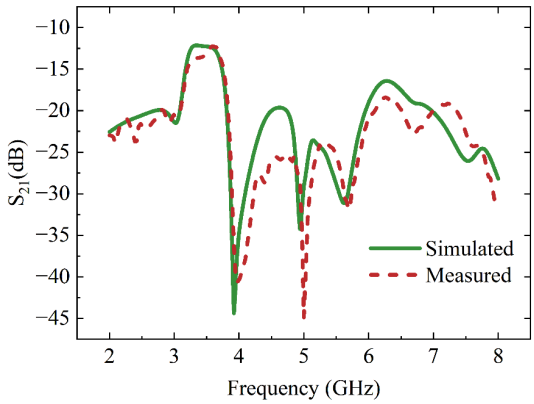

FIGURE 9. Simulated and measured mutual coupling between the diversity and main antennas, shown with S_{21}.

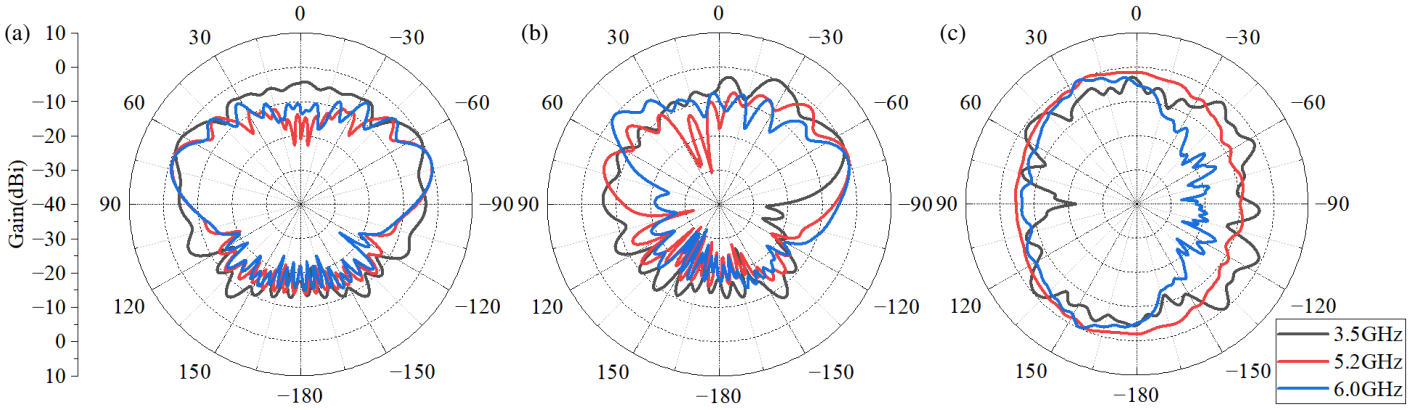

FIGURE 10. Simulated gain patterns at several frequencies on different planes of the proposed diversity antenna. (a) XOZ plane. (b) YOZ plane. (c) XOY plane.

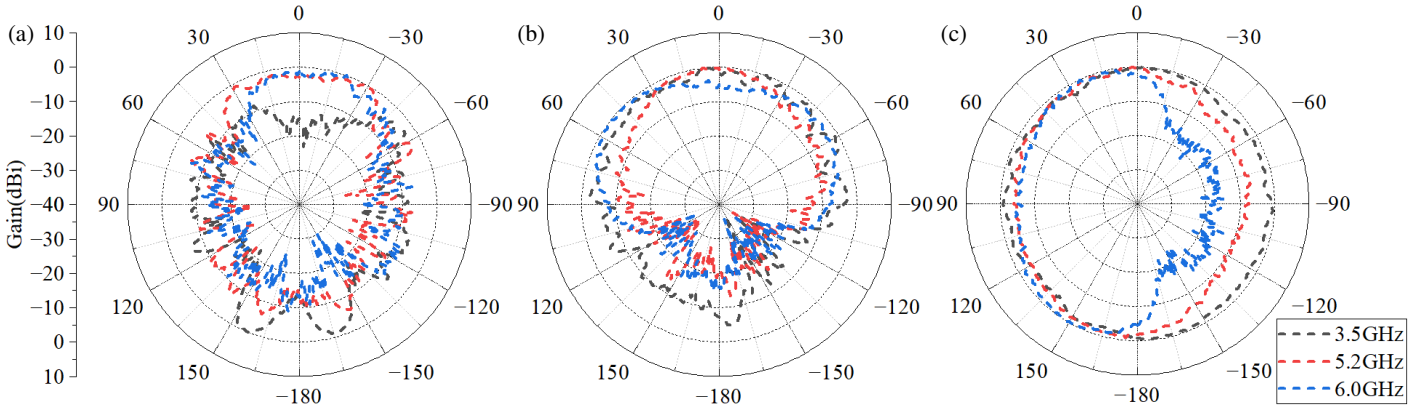

FIGURE 11. Measured gain patterns at several frequencies on different planes of the proposed diversity antenna. (a) XOZ plane. (b) YOZ plane. (c) XOY plane.

can be attributed to fabrication errors. Furthermore, as shown in Fig. 9, the isolation between the diversity and main antennas is better than 10 dB in both bands.

The simulated and measured far-field radiation patterns of the diversity antenna at 3 frequencies (3.5 GHz, 5.2 GHz, and 6.0 GHz) on the $XOZ/YOZ/XOY$ planes are shown in Fig. 10 and Fig. 11. It is seen that the radiation pattern of the radiating antenna is omnidirectional on the XOY plane. It is also noted that the pattern of the diversity antenna has a small back lobe due to the presence of the metal disc. Since the signal received by the car antenna may have a certain zenith angle with the car, it is necessary to maintain omnidirectionality at a certain zenith angle to ensure good signal reception. Overall, the proposed diversity antenna has good omnidirectionality in the horizontal plane at a certain elevation angle as shown in Fig. 12.

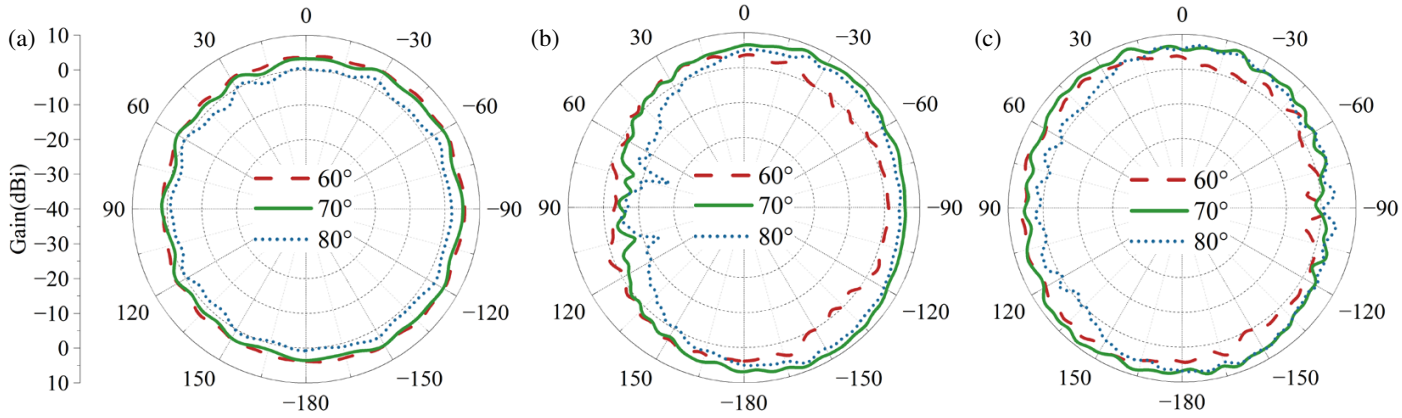

FIGURE 12. Simulated gain patterns at (a) 3.5 GHz, (b) 5.2 GHz and (c) 6.0 GHz on different elevation angles of the proposed diversity antenna.

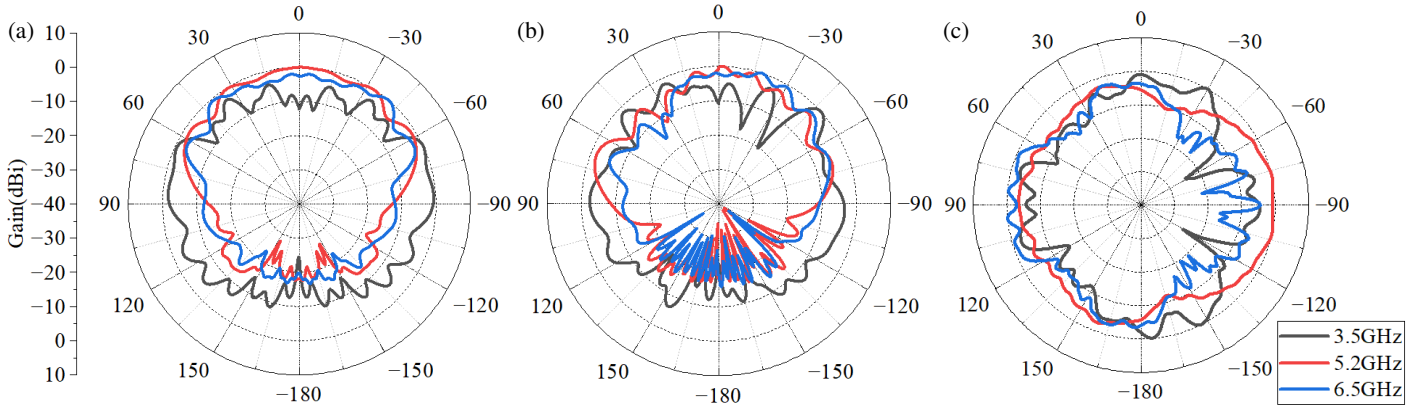

FIGURE 13. Simulated gain patterns at several frequencies on different planes of the proposed main antenna. (a) XOZ plane. (b) YOZ plane. (c) XOY plane.

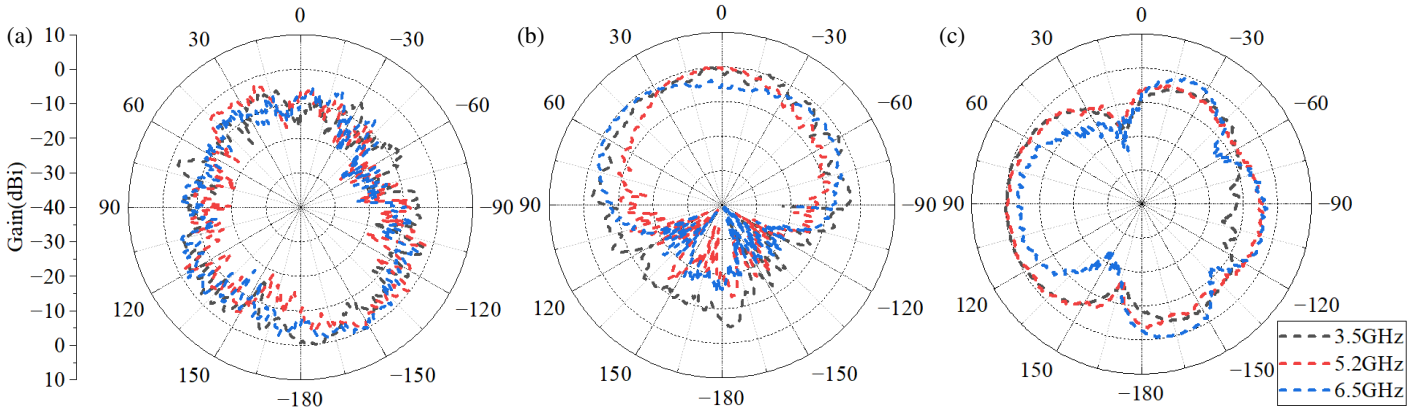

FIGURE 14. Measured gain patterns at several frequencies on different planes of the proposed main antenna. (a) XOZ plane. (b) YOZ plane. (c) XOY plane.

Figures 13 and 14 show the simulated and measured far-field radiation patterns of the main antenna at 3 frequencies (3.5 GHz, 5.2 GHz and 6.5 GHz) on the $XOZ/YOZ/XOY$ planes. The radiation pattern of the antenna can be observed to be omnidirectional in the XOY plane and exhibit an acceptable pattern in the XOZ/YOZ planes. Again, the pattern of the antenna has a small back lobe. Fig. 16 shows the measurement results of the horizontal plane radiation pattern at three points with different zenith angles (60°, 70°, 80°). It can be seen from Fig. 15 that the horizontal plane corresponding to three different elevation angles at different points has good omnidirectionality.

Figure 16 shows simulated radiation efficiency and gain. It can be seen that the efficiency of the main antenna is greater than 40% in both the low frequency band (3.35–3.75 GHz) and high frequency band (4.76–7.19 GHz). The corresponding gain of the main antenna is greater than 4 dBi in the whole operating frequency band. Meanwhile, the efficiency of the diversity antenna varies from 30% to 60% in the low frequency band

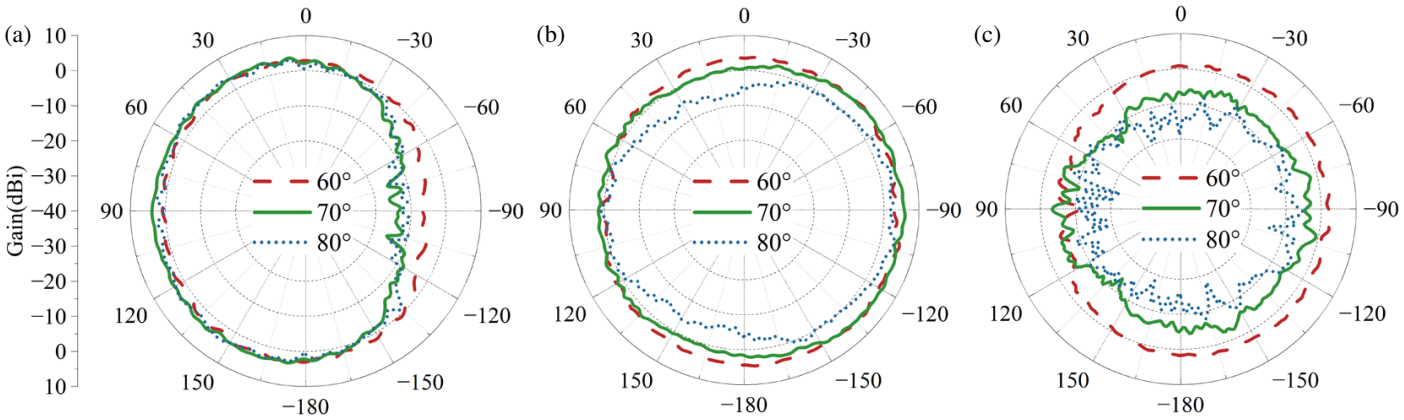

FIGURE 15. Simulated gain patterns at (a) 3.5 GHz, (b) 5.2 GHz and (c) 6.5 GHz on different elevation angles of the proposed main antenna.

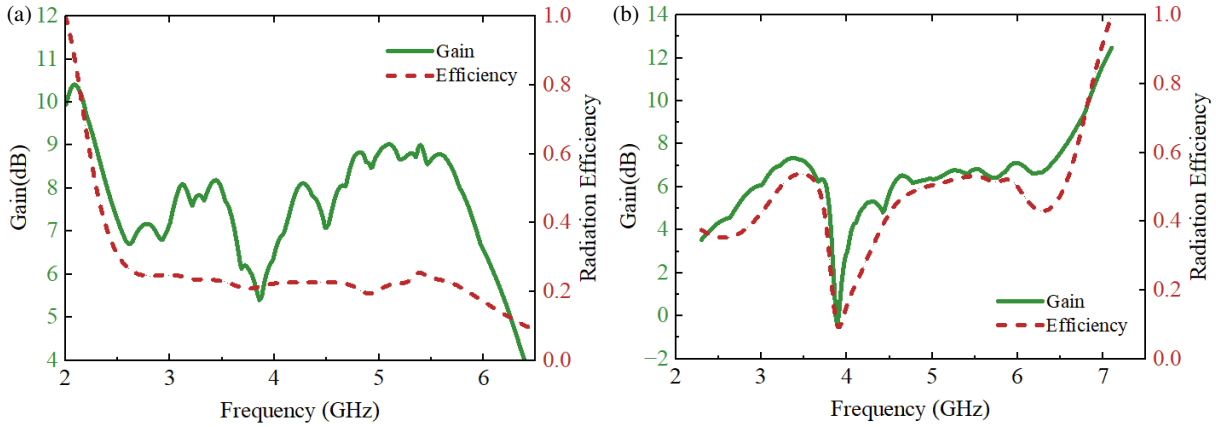

FIGURE 16. Simulated efficiency and gain of the (a) diversity antenna, (b) main antenna.

TABLE 2. A comparison of the proposed work with the designs in the literature.

Parameter	Bands	Dimension	Gain	Pattern
[7]	0.7 GHz, 1.2 GHz, 1.7 GHz, 2.2 GHz, 2.7 GHz	Height 99.5 mm	Not mentioned	Near omnidirectional
[8]	0.9 GHz, 2.0 GHz	Height 36 mm	−2.6 dBi @0.9 GHz	Semi-sphere
[11]	3.5 GHz	Height 60 mm	10.5 dBi	Not mentioned
[14]	0.85 GHz, 1.575 GHz, 2.4 GHz, 5.9 GHz	Height 73 mm	Not mentioned	Near omnidirectional
[20]	1.25 GHz–6 GHz	Length: 163 mm Height: 37 mm	>−10 dBi	For $\theta > 60°$, omnidirectional
[21]	1.8 GHz, 2.4 GHz 3.5 GHz, 5.85 GHz	Width: 75 mm Height: 52 mm	< 3 dBi	Near omnidirectional
[22]	4.82 GHz–6.67 GHz, 5.5 GHz	Diameter: 64 mm	6.5 dBi @5.5 GHz	Omnidirectional
This work	3.35–3.75 GHz, 4.76–7.19 GHz	In shark fin (height < 35 mm)	> 6 dBi for both bands	Omnidirectional

and from 31% to 60% for the high frequency band. The corresponding gain of the diversity antenna is about 0 dBi for low frequency bands and 1.6 to 6 dBi for high frequency bands. Given the small size of the antenna and the small effective radiation area, the gain of MIMO-LTE is acceptable [20].

A comparison between this work and other designs for vehicular applications is presented in Table 2. It is shown that this design has the advantage of omnidirectional radiation. The gain of this design is also satisfactorily high. For the dimension, the height of this design is only 35 mm, being compact enough in the consideration of its broadband and dual-antenna

nature. Lastly, the second band covered many applications. With the diversity and main antennas integrated into a single printed circuit board (PCB), this antenna has the potential of multi-functionalities.

4. CONCLUSION

In this article, a compact combination antenna for automotive applications is presented. The antenna is designed for shark fin-shaped housing on a car roof. To reduce the size and create sufficient bandwidth, deep learning method is used for optimization. Both antennas show satisfactory performance in the desired frequency band, covering two bands, including 3.35–3.75 GHz and 4.76–7.19 GHz. In addition, both antennas are 27 mm × 30 mm × 2 mm in size and require no matching network. Both the diversity and main antennas are compact designs with omnidirectional radiation patterns at a certain elevation angle.

ACKNOWLEDGEMENT

This work is funded in part by the Natural Science Foundation of Anhui Province (2308085Y02) and the National Natural Science Foundation of China (61871003).

REFERENCES

[1] Yang, F., S. Wang, J. Li, Z. Liu, and Q. Sun, "An overview of internet of vehicles," *China Communications*, Vol. 11, No. 10, 1–15, Oct. 2014.

[2] Ahmed, R. and F. H. Kumbhar, "VC3: A novel vehicular compatibility-based cooperative communication in 5G networks," *IEEE Wireless Communications Letters*, Vol. 10, No. 6, 1207–1211, Jun. 2021.

[3] Ullah, H., N. G. Nair, A. Moore, C. Nugent, P. Muschamp, and M. Cuevas, "5G communication: An overview of vehicle-to-everything, drones, and healthcare use-cases," *IEEE Access*, Vol. 7, 37 251–37 268, 2019.

[4] Masini, B. M., A. Bazzi, and A. Zanella, "A survey on the roadmap to mandate on board connectivity and enable V2V-based vehicular sensor networks," *Sensors*, Vol. 18, No. 7, 2207, Jul. 2018.

[5] Mao, C.-X., S. Gao, Y. Wang, Q. Luo, and Q.-X. Chu, "A shared-aperture dual-band dual-polarized filtering-antenna-array with improved frequency response," *IEEE Transactions on Antennas and Propagation*, Vol. 65, No. 4, 1836–1844, Apr. 2017.

[6] He, S. H., W. Shan, C. Fan, Z. C. Mo, F. H. Yang, and J. H. Chen, "An improved Vivaldi antenna for vehicular wireless communication systems," *IEEE Antennas and Wireless Propagation Letters*, Vol. 13, 1505–1508, 2014.

[7] Wu, Q., Y. Zhou, and S. Guo, "An L-sleeve L-monopole antenna fitting a shark-fin module for vehicular LTE, WLAN, and car-to-car communications," *IEEE Transactions on Vehicular Technology*, Vol. 67, No. 8, 7170–7180, Aug. 2018.

[8] Leelaratne, R. and R. Langley, "Multiband PIFA vehicle telematics antennas," *IEEE Transactions on Vehicular Technology*, Vol. 54, No. 2, 477–485, Mar. 2005.

[9] Oh, K., B. Kim, and J. Choi, "Novel integrated GPS/RKES/PCS antenna for vehicular application," *IEEE Microwave and Wireless Components Letters*, Vol. 15, No. 4, 244–246, Apr. 2005.

[10] Michel, A., P. Nepa, M. Gallo, I. Moro, A. P. Filisan, and D. Zamberlan, "Printed wideband antenna for LTE-band automotive applications," *IEEE Antennas and Wireless Propagation Letters*, Vol. 16, 1245–1248, 2017.

[11] Sreelakshmi, K., P. Bora, M. Mudaliar, Y. B. Dhanade, and B. T. P. Madhav, "Linear array Yagi-Uda 5G antenna for vehicular application," *International Journal of Engineering & Technology*, Vol. 7, No. 1.1, 513–517, 2018.

[12] Hastürkoğlu, S., M. Almarashli, and S. Lindenmeier, "A compact wideband terrestial MIMO-antenna set for 4G, 5G, WLAN and V2X and evaluation of its LTE-performance in an urban region," in *2019 13th European Conference on Antennas and Propagation (EuCAP)*, 1–5, Krakow, Poland, 2019.

[13] Chen, C., H. Gan, H.-L. Peng, C. Peng, G.-H. Xu, and J.-F. Mao, "High performance V2X antennas designed in integrated shark-fin environment," in *2020 International Conference on Microwave and Millimeter Wave Technology (ICMMT)*, 1–3, Shanghai, China, 20-23 2020.

[14] Kwon, O.-Y., R. Song, and B.-S. Kim, "A fully integrated shark-fin antenna for MIMO-LTE, GPS, WLAN, and WAVE applications," *IEEE Antennas and Wireless Propagation Letters*, Vol. 17, No. 4, 600–603, Apr. 2018.

[15] Zhou, W.-Y., Z.-l. Mei, M. Lu, and Y.-B. Zhu, "Deep learning for inverse design of broadband quasi-Yagi antenna," *International Journal of RF and Microwave Computer-Aided Engineering*, Vol. 2023, No. 1, 7819156, Feb. 2023.

[16] Sarker, N., P. Podder, M. R. H. Mondal, S. S. Shafin, and J. Kamruzzaman, "Applications of machine learning and deep learning in antenna design, optimization, and selection: A review," *IEEE Access*, Vol. 11, 103 890–103 915, Sep. 2023.

[17] Gadhafi, R., A. Copiaco, Y. Himeur, K. Afsari, H. Mukhtar, K. Ghanem, and W. Mansoor, "Exploring the potential of deep-learning and machine-learning in dual-band antenna design," *IEEE Open Journal of the Computer Society*, Vol. 5, 566–577, 2024.

[18] Peng, F. and X. Chen, "An antenna optimization framework based on deep reinforcement learning," *IEEE Transactions on Antennas and Propagation*, Vol. 72, No. 10, 7594–7605, Oct. 2024.

[19] Wu, D.-L., X. J. Hu, J. H. Chen, L. H. Ye, and J.-F. Li, "Ai deep learning optimization for compact dual-polarized high-isolation antenna using backpropagation algorithm," *IEEE Antennas and Wireless Propagation Letters*, Vol. 23, No. 2, 898–902, Feb. 2024.

[20] Artner, G., W. Kotterman, G. D. Galdo, and M. A. Hein, "Automotive antenna roof for cooperative connected driving," *IEEE Access*, Vol. 7, 20 083–20 090, Feb. 2019.

[21] Alsath, M. G. N. and M. Kanagasabai, "A shared-aperture multiservice antenna for automotive communications," *IEEE Antennas and Wireless Propagation Letters*, Vol. 13, 1417–1420, Jul. 2014.

[22] Wong, H., K. K. So, and X. Gao, "Bandwidth enhancement of a monopolar patch antenna with V-shaped slot for car-to-car and WLAN communications," *IEEE Transactions on Vehicular Technology*, Vol. 65, No. 3, 1130–1136, Mar. 2016.